

Article

Single-Source Precursors for Chemical Solution Deposition of Up-Converting NaLnF₄ Thin Films

Artem Shevchenko ^{1,2}, Andrei Anosov ^{1,2}, Daria Blinnikova ^{1,2}, Dmitry Grebenyuk ^{1,3}
and Dmitry Tsybarenko ^{1,*} 

¹ Department of Chemistry, Lomonosov Moscow State University, 119991 Moscow, Russia; shev.98@yandex.ru (A.S.); andrew_anosov.95@mail.ru (A.A.); d.blinnikovaa@gmail.com (D.B.); dimitrygrebenyuk@gmail.com (D.G.)

² Faculty of Materials Science, Lomonosov Moscow State University, 119991 Moscow, Russia

³ Faculty of Materials Science, MSU-BIT University, Shenzhen 518172, China

* Correspondence: tsymbarenko@gmail.com or tsymbarenko@inorg.chem.msu.ru

Abstract: Novel single-source precursors based on sodium and lanthanide pentafluoropropionates have been developed for chemical solution deposition of NaLnF₄ thin films (Ln = Y, Yb, Er, Tm). A series of [Ln₂(pfp)₆Q_n] (Q = H₂O, diglyme) and mixed-metal NaLn(pfp)₄Q_n were synthesized and characterized by X-ray diffraction (XRD) and thermogravimetric analysis (TG-DTA). Thermal decomposition of individual Na(pfp) and Ln(pfp)₃ occurs at different temperatures while single-source NaLn(pfp)₄ decomposes with the transformation to NaLnF₄ in a single stage at 280 °C. Further crystallization of NaLnF₄ was studied by variable-temperature powder XRD, which shows two phase transformations from cubic NaLnF₄ to hexagonal NaLnF₄ at 310 °C and back to a high-temperature cubic phase at 560 °C. The thin films of NaY_{0.78}Yb_{0.2}Er_{0.02}F₄ prepared by the dip-coating technique on Al₂O₃ substrates showed intense up-converting luminescence in green and blue regions under 980 nm excitation.

Keywords: single-source precursor; up-conversion; thin films; MOCSD; lanthanides; perfluorocarboxylates; fluorides; mixed-ligand complex; phase transition



Citation: Shevchenko, A.; Anosov, A.; Blinnikova, D.; Grebenyuk, D.; Tsybarenko, D. Single-Source Precursors for Chemical Solution Deposition of Up-Converting NaLnF₄ Thin Films. *Metals* **2022**, *12*, 488. <https://doi.org/10.3390/met12030488>

Academic Editors: Jordi Sort Viñas and Thomas Gries

Received: 9 February 2022

Accepted: 11 March 2022

Published: 14 March 2022

Publisher's Note: MDPI stays neutral with regard to jurisdictional claims in published maps and institutional affiliations.



Copyright: © 2022 by the authors. Licensee MDPI, Basel, Switzerland. This article is an open access article distributed under the terms and conditions of the Creative Commons Attribution (CC BY) license (<https://creativecommons.org/licenses/by/4.0/>).

1. Introduction

Sodium rare-earth fluorides have received much attention in the past decades, especially in the form of nanocrystals, because of their unique features: charge transfer and up-conversion luminescence (UCL) [1–4]. It is well known that NaYF₄ exists in cubic (α , fluorite type) or hexagonal (β , gagarinite type) modifications, and hexagonal β -NaYF₄ is considered to be the most effective host matrix for the Yb³⁺-Er³⁺ system, where the roles of the doping ions are sensibilization and activation, respectively [4,5]. Due to the exceptional chemical and thermal stability of metal fluorides, the formation of their thin films turns out to be a very challenging objective, requiring either high vacuum techniques [6,7] or a tricky electrochemical approach [8,9]. On the one hand, the corrosive effect of both elemental fluorine and fluoride ions makes already expensive physical vapor deposition techniques even more expensive by accelerated degradation of vacuum pumps, which renders the approach unpreferable. On the other hand, the electrochemically deposited fluoride films consist of 100% cubic NaYF₄ phase, which is a bad choice for optical applications. Chemical vapor deposition from metal organic precursors (MOCVD) is a robust method for smooth and homogeneous thin film fabrication at elevated temperatures. Recently, the concept of a third-generation single-source precursor with all necessary elements in one molecule has been proposed [10]. Volatile mixed-metal coordination compound [Na(tetraglyme)][Ln(hfa)₄] (hfa⁻ is hexafluoroacetylacetonate-anion) served as a source of fluorine atoms, and was successfully applied for the preparation of single-phase α -NaYF₄ thin film [10]. Another chemical method for thin film preparation is the metal-organic chemical solution deposition

(MOCSD), which in contrast to MOCVD allows for the precise control of cation composition of growing thin film that is essential for multi-component up-converting NaLnF_4 films, e.g., $\text{NaY}_{0.78}\text{Yb}_{0.20}\text{Er}_{0.02}$ [4,5]. Additionally, MOCSD is a simple and easily scalable technique; however, it requires a special design of metal-organic precursors. It has been reported that thermolysis of metal perfluorinated carboxylates (trifluoroacetates, pentafluoropropionates) also led to the formation of metal fluorides [11,12], which makes them valuable precursors for NaLnF_4 films and nanocrystals [13,14]. Mixed-ligand complexes, e.g., $[\text{Ln}_2(\text{tfa})_6(\text{diglyme})_2]$ [15,16] and $[\text{Ln}(\text{tfa})_2(\text{deta})_2](\text{tfa})$ [17], have been elaborated to modify the solubility and reactivity of precursors. Several polymeric single-source precursors for NaLnF_4 nanocrystals $[\text{NaLn}(\text{TFA})_4(\text{diglyme})]_\infty$ [18,19], $[\text{NaY}(\text{TFA})_4(\text{diglyme})]_\infty$, $[[\text{Na}(\text{triglyme})_2][\text{Y}_2(\text{TFA})_7(\text{THF})_2]]_\infty$ and $[\text{Na}_2\text{Y}(\text{TFA})_5(\text{tetraglyme})]_\infty$ [20] were also reported.

Here we present for the first time the development of a series of mono- and bimetallic precursors for MOCSD preparation of up-converting NaLnF_4 thin films based on metal pentafluoropropionates and a detailed study of the phase transformation during thermal treatment.

2. Materials and Methods

2.1. Synthesis of Metal Pentafluoropropionates

Rare earth and sodium carbonates (analytical grade, Reakhim, Moscow, Russia), pentafluoropropionic acid (Hpfp, 99%, P&M Invest, Moscow, Russia), diglyme (bis(2-methoxyethyl) ether, 99%, Fluka Honeywell, Charlotte, NC, USA) and isopropanol (Irea2000, Moscow, Russia, 99%) were used as received. Acetonitrile (Irea2000, Moscow, Russia, 99%) was preliminarily dried over P_2O_5 , distilled, and stored over 3\AA molecular sieves under argon.

$\text{Na}(\text{pfp})$ and $[\text{Ln}_2(\text{pfp})_6(\text{H}_2\text{O})_6]$ (**1Ln**) were prepared similarly to the reported method [17] from corresponding metal carbonate, which was placed into the glass beakers with deionized water and Hpfp with 10% excess to the stoichiometric amount was added dropwise. The mixture was stirred at room temperature until there was a complete dissolution of the carbonates and then recrystallized 3 times with the addition of extra water each time to get rid of remaining acid. Then, the solution was filtered using a PTFE Syringe filter (pore size $0.2\ \mu\text{m}$, Cole-Parmer, Vernon Hills, IL, USA) to remove the remaining particles and evaporated on a hot plate at $60\ ^\circ\text{C}$ until complete water removal. The purity of the resulting powders was confirmed by agreement of X-ray diffraction (XRD) and thermogravimetric analysis (TG-DTA) data with the previously reported ones [11,12].

Mixed-ligand complexes $[\text{Ln}_2(\text{pfp})_6(\text{diglyme})_2]$ (**2Ln**) were prepared using a Schlenk line from as-obtained pentafluoropropionate hydrates. Powder of $\text{Ln}(\text{pfp})_3(\text{H}_2\text{O})_3$ (0.56 mmol, ca. 0.4 g) was placed into a Schlenk flask and heated under vacuum at $110\ ^\circ\text{C}$ for 40 min. After cooling to room temperature, acetonitrile (2.5 mL) and diglyme (1.12 mmol, 0.161 mL) were added to the generated $\text{Ln}(\text{pfp})_3$ powder under vigorous stirring in Ar atmosphere. Then, the flask was heated to $90\ ^\circ\text{C}$ inside the Dewar vessel filled with hot water to obtain a clear solution and was left until it cooled naturally to room temperature, when crystalline precipitate was formed gradually. Yield: 70–80%.

2.2. NaLnF_4 Powders Preparation and VT-PXRD Study

Sodium and rare-earth pentafluoropropionates were dissolved in isopropanol for homogenization and then the solvent was evaporated until wet gel formation. After that, the samples were placed into a quartz boat and put into the furnace, where they were annealed at the desired temperatures. Samples for variable-temperature PXRD (VT-PXRD) measurements were prepared by thermal decomposition of single-source precursor at the lowest possible temperature ($240\text{--}250\ ^\circ\text{C}$) to obtain a poorly crystallized powder, which was then placed into corundum sample holder. The VT-PXRD experiment was performed on Rigaku SmartLab (Tokyo, Japan) using the Anton Paar HTK 1200 N chamber (Anton Paar, Graz, Austria) with a step temperature program ($10\ ^\circ\text{C}/\text{step}$) from room temperature to $600\ ^\circ\text{C}$. The full-profile Rietveld refinement of the XRD pattern at each certain temperature

was performed to determine the phase fraction and the sizes of the crystallites. The instrumental profile function was treated by a fundamental approach as implemented in Jana2006 software [21].

2.3. Precursor Solution Preparation and Thin Film Deposition

The precursor solution for thin film deposition was prepared by dissolving metal pentafluoropropionates in 5 mL isopropanol with the following cation ratio: $\text{Na}^+:\text{Y}^{3+}:\text{Yb}^{3+}:\text{Er}^{3+} = 100:78:20:2$ and concentration of the rare-earth elements $c(\text{Ln}) = 0.3$ M. After obtaining a clear solution, 1.5 mmol of diglyme was added dropwise during stirring. Metal carboxylate films were deposited on a single-crystal $c\text{-Al}_2\text{O}_3$ substrate implying the dip-coating technique with a pulling rate of 1 mm/s and a drying temperature of $T_d = 135$ °C. Then, the resulting amorphous precursor films were annealed at 400 and 600 °C for 15 min under argon with minor amounts of HF released from KHF_2 .

2.4. Methods and Instrumentation

XRD patterns were recorded on a Rigaku SmartLab diffractometer (Tokyo, Japan, $2\theta = 3\text{--}80^\circ$; $\text{Cu K}\alpha_1$ radiation) in $\theta\text{--}2\theta$ and grazing-incidence XRD (GIXRD, grazing angle was 0.5°) geometries. TG-DTA curves were obtained on Derivatograph Q-1500 D (MOM, Budapest, Hungary) in the static air condition with a heating rate of 10 °/min using the alumina crucible without a cap; the mass of the sample was 50 mg. Atomic force microscopy (AFM) was performed using NTEGRA Aura (NT-MDT, Moscow, Russia) in semicontact mode. The thickness of the films was determined by AFM profiling of artificial scratches on the film surface. The up-conversion luminescence (UCL) spectra were measured using the setup from a 980 nm diode laser with an average pumping power of 800 mW (Besram Technology Inc., Wuhan, China) and Ocean Optics USB2000 spectrometer (Orlando, FL, USA).

2.5. X-ray Crystallography

Single-crystal X-ray diffraction data were collected at 100K on a Bruker D8 QUEST (Incoatec micro-focus $\text{Mo K}\alpha$ X-ray tube, Photon III detector, Bruker AXS Inc., Madison, WI, USA) and Bruker Smart APEXII DUO (graphite monochromator, $\text{Mo K}\alpha$ X-ray tube, CCD detector, Bruker AXS Inc., Madison, WI, USA). Single crystals of **1Y** and **2Tm** were obtained by recrystallization of acetonitrile solution, and crystals of **3Ln** were collected after crystallization of precursor solution during 3 months. Absorption correction for **1Y** and **2Tm** crystals was performed using SADABS [22]. The crystal of **3Ln** was considered a two-component non-merohedral twin, which was detwinned using the CELL_NOW tool [23] and corrected for absorption by TWINABS [24]. Crystal structures were solved by direct methods and refined anisotropically for all non-H atoms with the full-matrix F^2 least-squares technique using SHELXTL PLUS [25]. H atoms of water molecules were localized from Fourier maps, other H-atoms were placed in idealized positions, and all H-atoms were refined in a riding model. Further details of the data collection and refinement are summarized in Table 1. CCDC reference number 2131909-2131911 contains the supplementary crystallographic data for this paper. These data can be obtained free of charge via <http://www.ccdc.cam.ac.uk/conts/retrieving.html> (accessed on 8 February 2022) (or from the CCDC, 12 Union Road, Cambridge CB2 1EZ, UK; Fax: +44 1223 336033; E-mail: deposit@ccdc.cam.ac.uk).

Table 1. Crystal and refinement data for the crystal structure **1Y**, **2Tm** and **3Ln**.

Compound	1Y	2Tm	3Ln
Formula	C ₁₈ H ₁₂ F ₃₀ O ₁₈ Y ₂	C ₃₀ H ₂₈ F ₃₀ O ₁₈ Tm ₂	C ₄₅ H ₂₄ F ₅₅ Na ₇ O ₃₁ Y _{1.56} Yb _{0.40} Er _{0.04}
Formula weight	1264.10	1584.38	2481.18
Diffractometer	Bruker D8 QUEST	Bruker Smart APEX DUO	Bruker D8 QUEST
Data collection method	ω-scans	ω-scans	ω-scans
Temperature (K)	100(2)	120(2)	150(2)
Crystal system	Triclinic	Monoclinic	Triclinic
Space group	<i>P1</i> [−]	<i>P2</i> ₁ / <i>c</i>	<i>P1</i> [−]
<i>a</i> (Å)	9.062(4)	12.036(2)	12.8526(12)
<i>b</i> (Å)	10.202(5)	18.553(3)	14.7852(13)
<i>c</i> (Å)	11.113(6)	12.084(2)	23.055(2)
<i>α</i> (°)	90.78(2)	90	100.753(2)
<i>β</i> (°)	110.03(2)	113.849(3)	101.520(2)
<i>γ</i> (°)	106.05(2)	90	91.705(2)
<i>V</i> (Å ³)	921.0(8)	2468.1(7)	4207.3(7)
<i>Z</i>	1	2	2
Color, habit	Colorless, plate	Colorless, plate	Colorless, block
Crystal dimensions (mm)	0.24 × 0.17 × 0.06	0.31 × 0.30 × 0.12	0.269 × 0.172 × 0.097
<i>D</i> _{calc} (g·cm ^{−3})	2.279	2.132	1.959
<i>μ</i> (mm ^{−1})	3.360	3.751	1.785
Unique reflections (<i>R</i> _{int})	4731 (0.1108)	5948 (0.0499)	18,172 (0.1015)
Observed reflections [<i>I</i> > 2σ(<i>I</i>)]	3327	4324	9391
Parameters, restraints	307, 0	363, 0	1262, 179
<i>R</i> ₁ [<i>I</i> > 2σ(<i>I</i>)], ω <i>R</i> ₂	0.0704, 0.1700	0.0349, 0.0790	0.0901, 0.2755
Goodness-of-fit on <i>F</i> ²	1.039	1.066	1.020
Absorption correction	SADABS	SADABS	TWINABS
<i>T</i> _{min} , <i>T</i> _{max}	0.499, 0.824	0.2543, 0.6593	0.5359, 0.7455
<i>ρ</i> _{min} , <i>ρ</i> _{max} (eÅ ^{−3})	−1.529, 1.861	−1.923, 1.996	−0.860, 1.808

3. Results and Discussion

3.1. Synthesis and Thermal Behavior of Single-Source Precursors

Powders of sodium and lanthanide pentafluoropropionates isolated from water solution are well soluble in alcohols (methanol, isopropanol, etc.). Crystallization from isopropanol solutions of individual [Na(pfp)] or [Ln₂(pfp)₆(H₂O)₆] (**1Ln**) yields the well-crystalline powders (Figure 1) with compositions similar to as-obtained ones and with Powder XRD (PXRD) patterns being in a good agreement with the theoretical patterns calculated from the single-crystal structures of Na(pfp) [12] and [Y₂(pfp)₆(H₂O)₆] (**1Y**). One should note the extra peak at a small angle in experimental PXRD of **1Y** that corresponds to the by-product phase, which forms tiny needle-like crystals unsuitable for X-ray structure analysis. More importantly, crystallization of a solution containing both [Na(pfp)] and **1Ln** simultaneously leads to the formation of a novel bimetallic complex NaY(pfp)₄(H₂O)₃. The unique PXRD pattern of the NaY(pfp)₄(H₂O)₃ sample contains no peaks originating from the patterns of individual [Na(pfp)] or **1Ln** phases, which confirms the formation of a single phase with an entirely new crystal structure (Figure 1).

The formation of a single-source bimetallic complex significantly affected the thermal behavior of the precursors. Indeed, the individual [Na(pfp)] or **1Ln** phases totally decomposed with the formation of metal fluorides at remarkably different temperatures, 260 and 300 °C, respectively (Figure 2). This feature along with impeded diffusion at low temperatures increased the risk of formation of the final material in the form of disintegrated NaF and YF₃ grains.

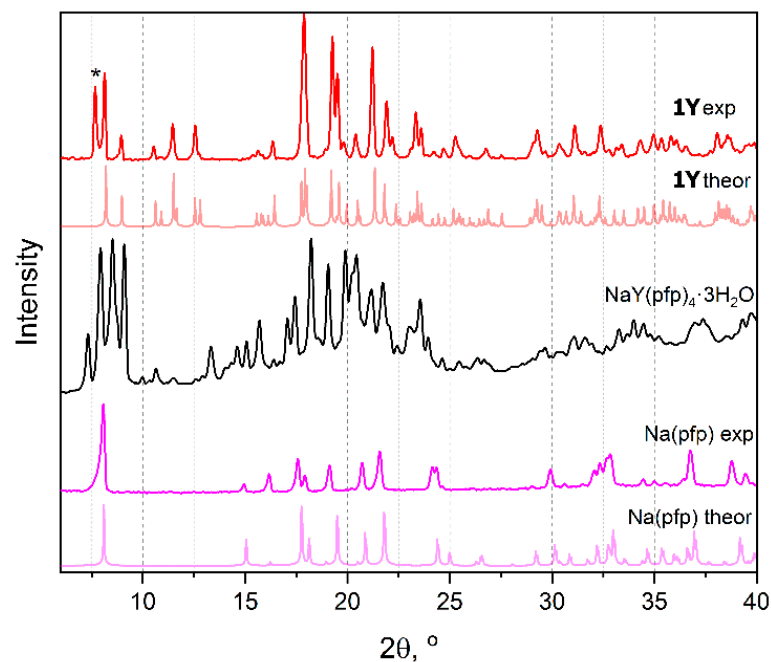


Figure 1. Calculated and experimental PXRD patterns of $[Y_2(pfp)_6(H_2O)_6]$ (**1Y**), $Na(pfp)$ and $[NaY(pfp)_4(H_2O)_3]$ (black). Symbol * indicates the peak of the by-product phase of $Y(pfp)_3 \cdot nH_2O$ with a polymeric structure.

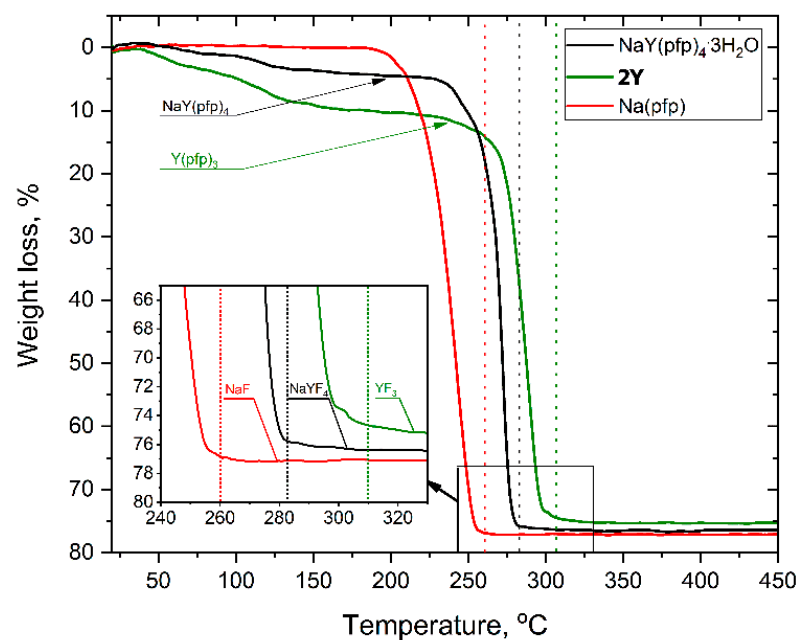


Figure 2. TG-curves for the thermal decomposition of individual and heterometallic pentafluoropropionates heated at $10^\circ/\text{min}$ in air atmosphere. Vertical dotted lines correspond to the end of thermal decomposition.

Thermal decomposition of $NaY(pfp)_4(H_2O)_3$ occurs in two stages (Figure 2). The first preliminary stage of weight loss ($70\text{--}170^\circ\text{C}$) corresponds to the elimination of three water molecules (calc—6.6 %, found—5.4 %), resulting in an anhydrous $NaY(pfp)_4$. The later one decomposes at the second stage in a narrow temperature range of $240\text{--}280^\circ\text{C}$ with the formation of pure $NaYF_4$ (calc. total weight loss—77.0%, found—76.4%), which was confirmed by the PXRD of the residue. It should be noted that total decomposition

temperature of $\text{NaY}(\text{pfp})_4$, ca. $283\text{ }^\circ\text{C}$, is close to the median value between $\text{Na}(\text{pfp})$ and $\text{Y}(\text{pfp})_3$.

The use of the elaborated compounds as single-source precursors for fluoride thin film deposition is very convenient since the cationic ratio of rare-earth elements could be easily controlled by dissolving various amounts of powder precursors, which is very important for optical and magnetic applications. Moreover, deposition from the solution provides a homogeneous distribution of elements only if there would be no place for crystallization on the substrate during the drying stage. The ability to form well-crystalline powder most probably originates from the relatively large lattice energy of $\text{Na}(\text{pfp})$ and **1Ln** polymeric crystal structures, and from the additional framework of intermolecular hydrogen bonds in **1Ln**. In order to modify the composition and structure of complexes in solution and to prevent their crystallization, the gel-stabilizer, diglyme, was added to isopropanol or acetonitrile precursor solutions. The ability of diglyme to coordinate the Ln atom as a chelating and bridging ligand and to form mixed-ligand complexes preserves such a solution from crystallization on the substrate, but at the same time, it diminishes the opportunity of structure determination of the single-source precursor [26]. However, in the anhydrous conditions of the Schlenk apparatus, the crystalline products of $[\text{Ln}_2(\text{pfp})_6(\text{diglyme})_2]$ complexes (**2Ln**), Ln = Y, Er, Tm, Yb, were isolated from acetonitrile solution of $\text{Ln}(\text{pfp})_3$ and diglyme and were found to be isostructural to a **2Tm** analog whose crystal structure was determined (Figure 3). By contrast, the mixed-metal precursor solution of $\text{Na}(\text{pfp})$, $\text{Ln}(\text{pfp})_3$ and diglyme forms a very viscous clear gel without any crystalline product during solvent evaporation. Thus, the crystallization of the later one became only possible due to the partial degradation of the ligands, which resulted in the formation of poorly soluble polymeric compounds. Indeed, the storage of precursor solution based on Na, Y, Yb and Er pentafluoropropionates with diglyme after three months led to the formation of a few X-ray quality single crystals of coordination polymer $[\text{Na}_7\text{Ln}_2(\text{pfp})_{11}(\text{form})(\text{diglyme})(\text{Meac})]_\infty$ (**3Ln**), where form^- , (HCOO^-) and Meac^- ($\text{MeOC}_2\text{H}_4\text{OCH}_2\text{COO}^-$) anions were formed due to degradation of pfp^- and diglyme ligands.

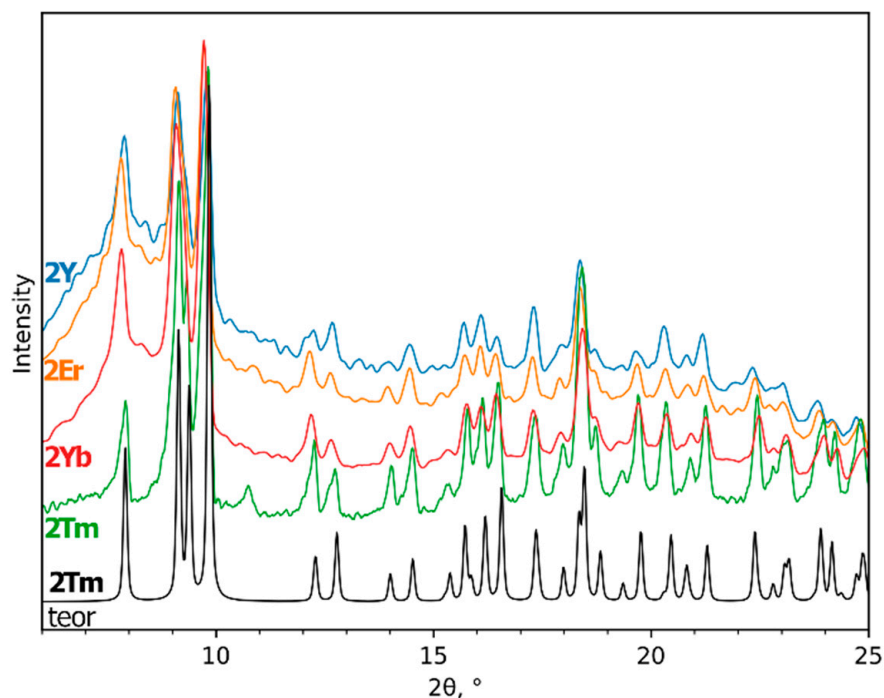


Figure 3. Experimental PXRD patterns of $[\text{Ln}_2(\text{pfp})_6(\text{diglyme})_2]$ (**2Ln**, Ln = Y, Er, Tm, Yb) and theoretical PXRD pattern of **2Tm** at room temperature.

3.2. Crystal Structure

3.2.1. $[\text{Ln}_2(\text{pfp})_6(\text{H}_2\text{O})_6]$ ($\text{Ln} = \text{Y}, \text{Er}, \text{Tm}, \text{Yb}$) (**1Ln**)

Crystal structure of **1Ln** series was determined for Y analog (**1Y**) by single-crystal XRD. The triclinic unit cell contains centrosymmetric binuclear $[\text{Y}_2(\text{pfp})_6(\text{H}_2\text{O})_6]$ molecules (Figure 4). The Y cation is coordinated by three O atoms from water molecules, four O atoms of four bridging pfp[−] anions and one O atom of terminal pentafluoropropionate anion (Table 2). Thus, the coordination number (CN) of Y equals to 8 and the environment is best described as a distorted double-capped trigonal prism. The $\text{Y}\cdots\text{Y}^i$ distance is 4.520 Å, which is common for other binuclear complexes of rare-earth elements. Binuclear molecules of **1Y** are packed parallel to each other in the *ab* plane (Figure 5). The framework of H-bonds defines the mutual orientation of molecules within the layer. The structure of **1Y** is isotypic to previously reported Gd analog [27], while the Y–O distances are 0.04–0.06 Å shorter than Gd–O ones due to the smaller ionic radius of Y cation.

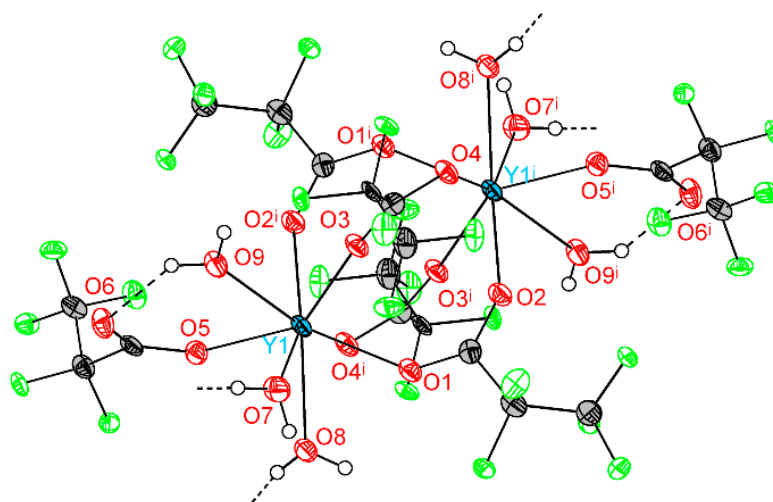


Figure 4. Molecular geometry in **1Y** structure. Y atoms are depicted at 50% probability, light atoms at 30% probability. Colour code: Y, cyan; O, red; F, green; C, grey; H, white. H atoms are omitted partially for clarity. Symmetry code (i): $-x, 1 - y, 1 - z$.

Table 2. Selected interatomic distances (Å) in **1Y**. Symmetry code (i): $1 - x, 1 - y, 2 - z$.

Parameter	Distance
Ln1–O1	2.293(4)
Ln1–O2 ⁱ	2.306(4)
Ln1–O3	2.322(4)
Ln1–O5	2.312(4)
Ln1–O4 ⁱ	2.383(4)
Ln1–O7	2.339(4)
Ln1–O8	2.411(4)
Ln1–O9	2.339(4)
Ln1 \cdots Ln1 ⁱ	4.483(2)
D \cdots A distance in hydrogen bonds	
O7–H1 \cdots O6 ⁱⁱ	2.721(5)
O8–H3 \cdots O4 ⁱⁱⁱ	2.873(7)
O9–H6 \cdots O6	2.629(6)

Symmetry codes: (i) $-x, 1 - y, 1 - z$; (ii) $1 - x, 2 - y, 1 - z$; (iii) $1 - x, y, z$.

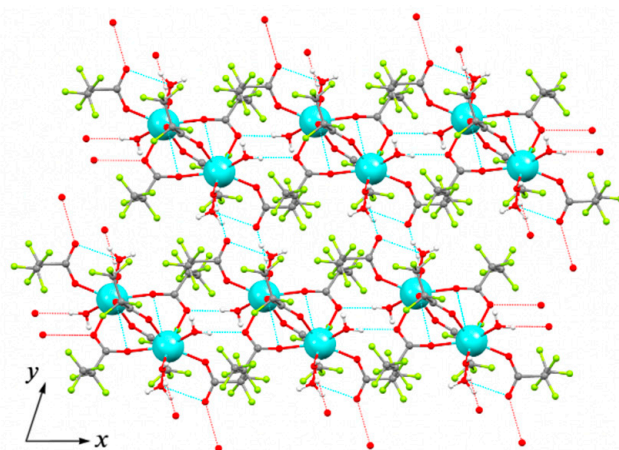


Figure 5. Topology of layer in *ab* plane formed by molecular species in crystal structure of **1Y**. Colour code: Y, cyan; O, red; F, green; C, grey. H atoms are omitted for clarity. Dashed lines show H-bonds.

3.2.2. $[\text{Ln}_2(\text{pfp})_6(\text{diglyme})_2]$, (Ln = Y, Er, Tm, Yb) (**2Ln**)

Crystal structure of **2Ln** series was determined for Tm analog. The monoclinic unit cell contains two symmetrically related centrosymmetric binuclear molecules of $[\text{Tm}_2(\text{pfp})_6(\text{diglyme})_2]$ (Figure 6). Tm atom with CN equal to 8 is coordinated by O1, O5, O2ⁱ and O6ⁱ atoms of four bridging pfp[−] anions, one O3 atom of a terminal pfp[−] anion, and O7, O8 and O9 atoms of the chelating diglyme ligand (Table 3). The coordination polyhedron of Tm is best described as a distorted double-capped trigonal prism.

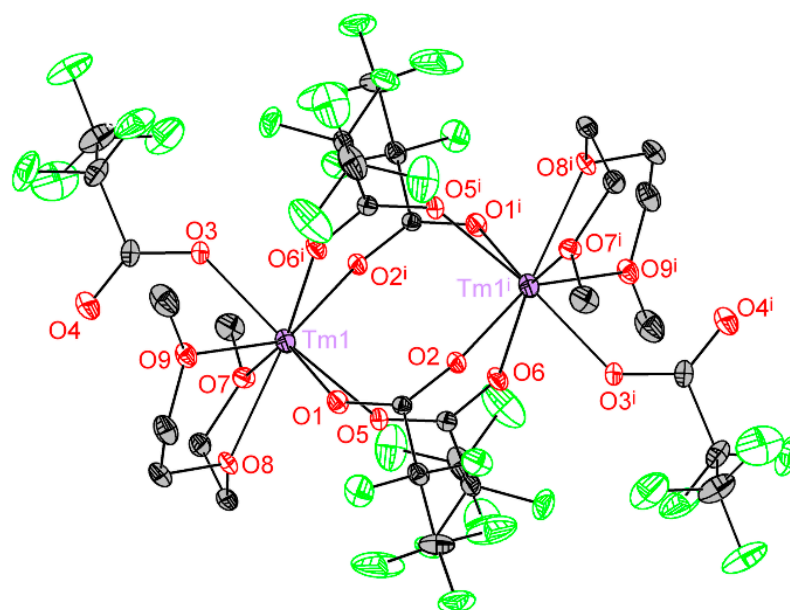


Figure 6. $\text{Tm}_2(\text{pfp})_6(\text{diglyme})_2$ binuclear molecule. Tm atoms are depicted at 50% probability, light atoms at 30% probability. Colour code: Tm, violet; O, red; F, green; C, grey. H atoms are omitted for clarity. Symmetry code (i): $1 - x, 1 - y, 2 - z$.

Therefore, the molecular structure of **2Tm** is very similar to that in the **1Y** structure, where H_2O molecules are replaced with three donor atoms of diglyme ligand. By contrast to **1Y**, the diglyme in **2Tm** prevents the formation of an H-bonds framework and results in the packing of isolated binuclear molecules in a pseudo-hexagonal motif within the *bc* plane (pseudo-hexagonal cell parameter $\gamma_h = 121.63^\circ$, Figure 7). Comparison of **2Tm** with the previously reported isotypic $[\text{Ln}_2(\text{tfa})_6(\text{diglyme})_2]$ (Ln = Gd, Tm, Yb) trifluoroacetate analog [15] reveals the interatomic distances in **2Tm** to be 0.01–0.03 Å larger

than in $\text{Tm}_2(\text{tfa})_6(\text{diglyme})_2$, which is attributed to the increase in steric hindrance with bulky pfp^- ligands. Additionally, in contrast to **2Tm**, the pseudo-hexagonal motif of $\text{Tm}_2(\text{tfa})_6(\text{diglyme})_2$ packing cannot be recognized.

Table 3. Selected interatomic distances (Å) in **2Tm**. Symmetry code (i): $1 - x, 1 - y, 2 - z$.

Parameter	2Tm
Tm1–O1	2.343(4)
Tm1–O2 ⁱ	2.278(4)
Tm1–O3	2.245(3)
Tm1–O5	2.304(3)
Tm1–O6 ⁱ	2.279(3)
Tm1–O7	2.432(3)
Tm1–O8	2.399(3)
Tm1–O9	2.405(3)
Tm1...Tm1 ⁱ	4.5199(6)

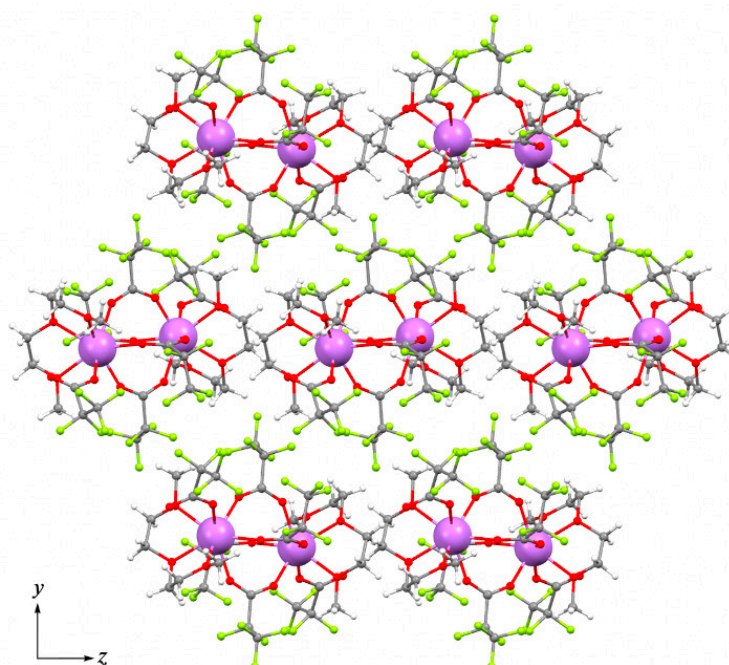


Figure 7. Packing diagram of $[\text{Tm}_2(\text{pfp})_6(\text{diglyme})_2]$ molecules within bc plane in structure **2Tm**. Colour code: Tm, violet; O, red; F, green; C, grey; H, white.

3.2.3. $[\text{Na}_7\text{Ln}_2(\text{pfp})_{11}(\text{form})(\text{diglyme})(\text{Meac})]_\infty$ (Ln = Y, Er, Yb) (**3Ln**)

The single crystals of the mixed-metal compound **3Ln** were harvested from the gel-like mother liquor formed after solvent evaporation from the mixed-metal precursor solution of $[\text{Na}(\text{pfp})]$ and $[\text{Ln}_2(\text{pfp})_6(\text{H}_2\text{O})_6]$, where $\text{Ln} = \text{Y}_{0.78}\text{Yb}_{0.20}\text{Er}_{0.02}$; the same cation ratio was set up for Ln ions in the **3Ln** structure. The asymmetric part of the triclinic unit cell contains seven Na atoms, two Ln atoms, eleven pfp^- anions, one diglyme ligand and additionally form^- and Meac^- anions. The **3Ln** compound possesses a layered structure. Layers are formed due to the linking of the 1D polymeric $\{\text{Na}_5(\text{pfp})_5\}_\infty$ species and tetranuclear heterometallic $\{\text{Na}_2\text{Ln}_2(\text{diglyme})(\text{Meac})(\text{pfp})_6(\text{form})\}$ species via the bridging functions of Meac^- and pfp^- anions.

In tetranuclear species each cation, Ln1, Ln2, Na6, and Na7, exhibits a unique coordination environment (Figure 8, Table 4). The coordination environment of the Na6 cation is formed by chelating form^- anion (O27, O28) and O17, O19 and O21 atoms of three bridging pfp^- anions, while the Na7 cation is coordinated by the same O17 and O21 atoms of two pfp^- anions and additionally by chelating neutral diglyme ligand (O29, O30 and

O31). Ln1 with a pentagonal bipyramidal environment (CN equals to 7) is coordinated by O2, O8, O16, O18, O20 and O23 atoms of six bridging pfp[−] anions and by O28 atom of chelato-bridging form[−] anion from the Na6 environment. Ln2, being in a triangular dodecahedral environment with CN equal to 8, is coordinated by O6ⁱ, O10ⁱ, O14ⁱ and O22 atoms of four bridging pfp[−] anions, by O27 atom of form[−] anion and by O24ⁱ, O25ⁱ and O26ⁱ atoms of chelating Meac[−] anion.

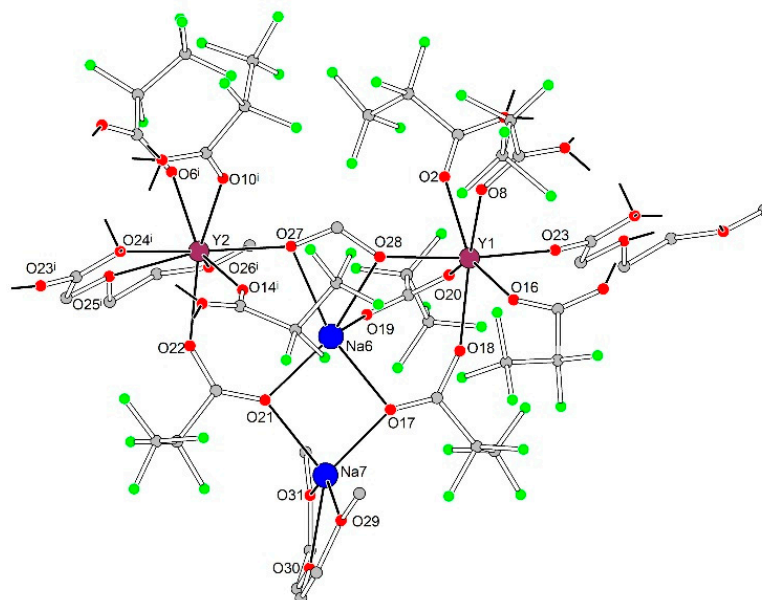


Figure 8. Geometry of $\{\text{Na}_2\text{Ln}_2(\text{diglyme})(\text{Meac})(\text{pfp})_6(\text{form})\}$ species in the crystal structure of **3Ln**. Colour code: Y | Yb | Er, burgundy; Na, blue; O, red; F, green; C, grey. H-atoms are omitted for clarity.

Table 4. Selected interatomic distances (Å) in **3Ln** structure. Symmetry codes: (i) $x - 1, y, z$; (ii) $2 - x, -y, 2 - z$; (iii) $2 - x, -y, 1 - z$.

Parameter	Distance	Parameter	Distance	Parameter	Distance	Parameter	Distance	Parameter	Distance
Distances in 1D polymeric $\{\text{Na}_5(\text{pfp})_5\}_\infty$ species									
Na1–O1	2.352(9)	Na2–O1	2.621(9)	Na3–O4	2.338(7)	Na4–O7	2.381(8)	Na5–O12	2.324(11)
Na1–O3	2.345(10)	Na2–O4	2.352(9)	Na3–O7	2.408(9)	Na4–O9	2.455(8)	Na5–O13	2.315(12)
Na1–O3 ⁱⁱ	2.284(8)	Na2–O5	2.307(10)	Na3–O9	2.326(9)	Na4–O11	2.429(10)	Na5–O12 ⁱⁱⁱ	2.291(8)
Na1–O5	2.373(9)	Na2–O7	2.409(9)	Na3–O11	2.318(8)	Na4–O13	2.287(10)	Na5–O15	2.352(10)
Na1–F2	2.699(11)	Na2–O9	2.370(8)	Na3–F8	2.602(9)	Na4–O15	2.319(9)	Na5–F26 ⁱⁱⁱ	2.617(10)
Na1–F7 ⁱⁱ	2.639(10)	Na2–O24	2.287(9)	Na3–F16	2.478(11)	Na4–O23	2.871(9)	Na5–F31	2.879(15)
Na1–F11	2.678(12)	-	-	Na3–F21	2.767(10)	Na4–O24	2.498(9)	Na5–F37	2.817(14)
-	-	-	-	Na3–F28	2.558(11)	-	-	-	-
Distances in tetranuclear heterometallic $\{\text{Na}_2\text{Ln}_2(\text{diglyme})(\text{Meac})(\text{pfp})_6(\text{form})\}$ species									
Na6–O17	2.288(11)	Na7–O17	2.233(12)	Y1–O2	2.266(8)	Y2–O6 ⁱ	2.300(7)	-	-
Na6–O19	2.34(2)	Na7–O21	2.318(11)	Y1–O8	2.311(11)	Y2–O10 ⁱ	2.319(9)	-	-
Na6–O21	2.262(10)	Na7–O29	2.31(2)	Y1–O16	2.267(9)	Y2–O14 ⁱ	2.282(10)	-	-
Na6–O27	2.402(12)	Na7–O30	2.289(18)	Y1–O18	2.252(11)	Y2–O22	2.291(9)	-	-
Na6–O28	2.374(12)	Na7–O31	2.39(2)	Y1–O20	2.334(12)	Y2–O24 ⁱ	2.325(8)	-	-
-	-	Na7–F51	2.938(12)	Y1–O23	2.226(8)	Y2–O26 ⁱ	2.429(12)	-	-
-	-	-	-	Y1–O28	2.229(8)	Y2–O27	2.259(8)	-	-

The 1D polymeric $\{\text{Na}_5(\text{pfp})_5\}_\infty$ species in **3Ln** contains Na1–Na5 cations with coordination environments of three types (Figure 9). Na1 and Na5 cations, both with CN equal to 4 + 3, are coordinated by four O-atoms of four bridging pfp[−] anions, and by three additional F-atoms of $-\text{CF}_2-$ groups from coordinated pfp[−]. The coordination environment of Na2 and Na4 cations is formed by six O-atoms of six bridging pfp[−] anions. Finally, the Na3 cation with CN equal to 4 + 4 is coordinated by O4, O7, O9 and O11 atoms of four pfp[−] anions as well as by F8, F16, F21 and F28 of the same pfp[−] anions. One can virtually separate

the polymeric $\{Na_5(pfp)_5\}_\infty$ species into several corner-shared and face-shared binuclear building blocks with square $\{Na_2O_2\}$ and trigonal bipyramidal $\{Na_2O_3\}$ metal-oxygen cores, which were recently considered to be the most energetically favorable for Na-based coordination polymers [28]. The $\{Na_5(pfp)_5\}_\infty$ chains act as ‘guide rods’ assembling the structure to 2D layers via bridging tetranuclear heterometallic $\{Na_2Ln_2(diglyme)(Meac)(pfp)_6(form)\}$ species (Figure 10). A similar feature was recently revealed by us for the 3D dense coordination polymer $[HKCu_2(prop)_6]_\infty$ with non-fluorinated propionate ligands, where $[HK(prop)_2]_\infty$ chains were linked into a framework via binuclear $[Cu_2(prop)_4]$ paddle-wheel units [29]. One could expect a similar 3D structure for **3Ln**, since Ln^{3+} ions also tend to form coordination polymers even with bulky anionic ligands [30–32]. However, simultaneous coordination of polydentate diglyme and $Meac^-$ ligands along with bulky $-C_2F_5$ groups of pfp^- anions effectively shielded Ln^{3+} and Na^+ cations and resulted in a 2D coordination polymer.

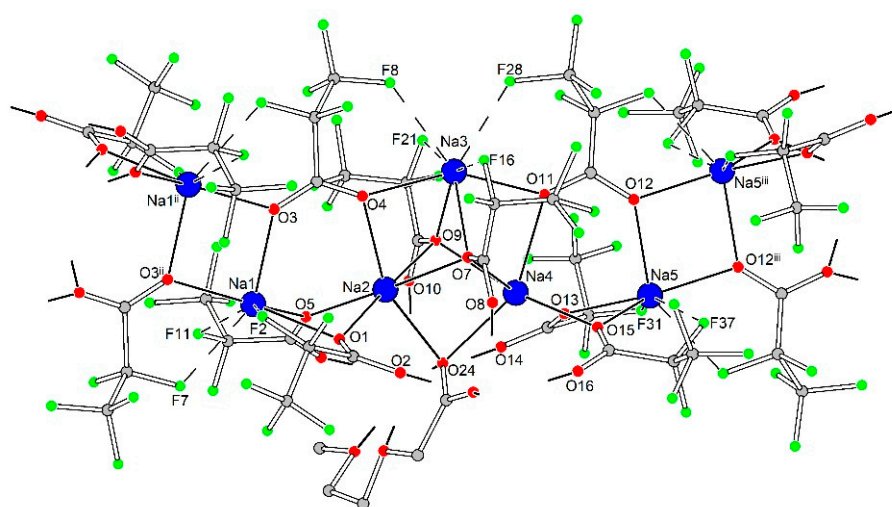


Figure 9. Geometry of 1D polymeric $\{Na_5(pfp)_5\}_\infty$ species in the crystal structure of **3Ln**. Colour code: Na, blue; O, red; F, green; C, grey. H-atoms are omitted for clarity. Dash lines show $Na \cdots F$ contacts.

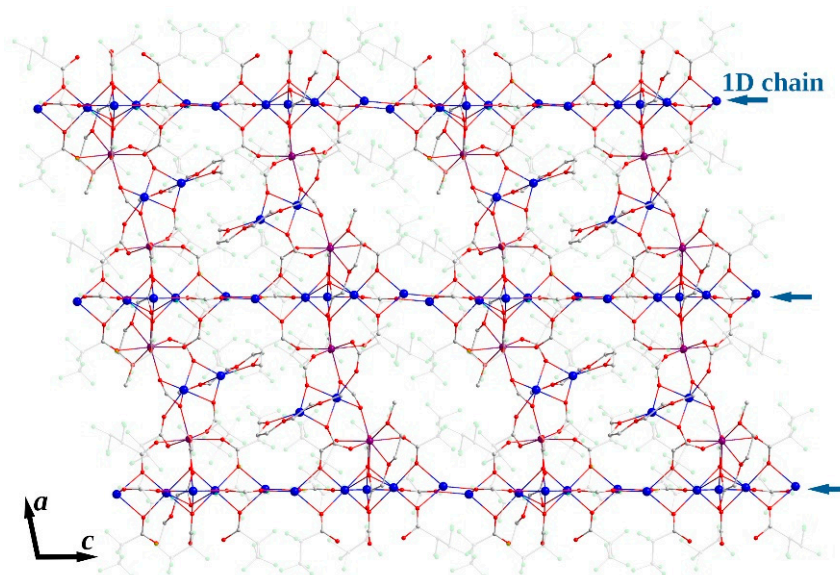


Figure 10. Topology of 2D layer in crystal structure of **3Ln**. Colour code: Y | Yb | Er, burgundy; Na, blue; O, red; F, green; C, grey. Perfluoroethyl groups of pfp^- anions are depicted in semitransparent mode. H-atoms are omitted for clarity.

3.3. NaLnF₄ Powders Preparation and Characterization

The high reactivity of perfluorinated precursors allows one to perform the chemical synthesis of NaLnF₄ at temperatures as low as 300–400 °C. According to the phase diagram of the NaF–YF₃ system, this should lead to the formation of hexagonal β-NaLnF₄, which is stable up to 680–690 °C [33] and is considered the most suitable for UCL application [34]. However, weak diffusion during low temperature synthesis often leads to crystallization of the disordered cubic α-NaLnF₄ phase of the fluorite type. Thus, the crystallization process of NaLnF₄ prepared from the thermal decomposition of metal carboxylate precursors was studied by VT-PXRD (Figure 11).

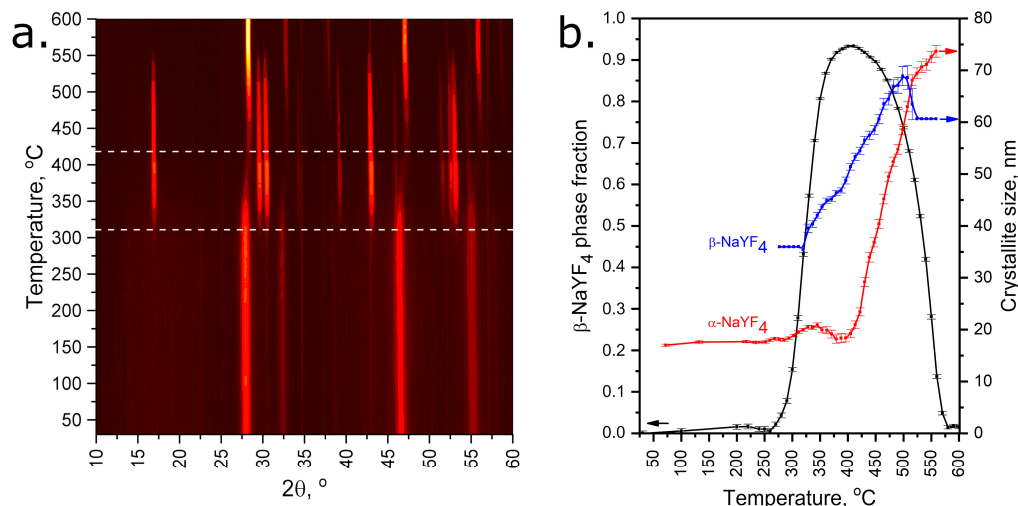


Figure 11. VT-PXRD patterns of as-obtained NaYF₄ (a) and result of Rietveld refinement (b). Horizontal dashed lines at 310 and 420 °C correspond to the beginning of the crystallization process of the hexagonal and cubic phases, respectively. XRD patterns recorded at 270–320 °C and 560–600 °C temperature ranges were refined with a fixed crystallite size of β-NaYF₄ due to its minor content.

According to the VT-PXRD data, two phase transformations of as-obtained NaYF₄ occur in a temperature range of 25–600 °C. At 25–310 °C, the as-obtained sample contains almost pure metastable cubic α-NaYF₄ phase with minor contents of a hexagonal β-NaYF₄ one within the agreement with Ostwald’s step rule [35]. One can notice the broad peaks of α-NaYF₄ at the lower temperatures, which confirms the poor crystallinity of the sample with an estimated crystallite size of less than 20 nm. Further heating activates the ion diffusion effects, and after 310 °C the cubic phase remarkably transforms into the thermodynamically stable hexagonal phase. This process also increases crystallinity, and the size of hexagonal crystallites increases to 70 nm. The maximum amount of hexagonal phase is observed in the 400–440 °C temperature range; however, traces of cubic phase still remain in the sample. Finally, further heating leads to the transformation of the hexagonal phase back to the high-temperature cubic phase with high crystallinity.

3.4. NaLnF₄ Thin Films

The metal organic precursors described above were used for the deposition of complex fluoride thin films by MOCSD. At the first stage, a gel-like amorphous film is formed by the dip-coating technique from homogeneous precursor solution after solvent evaporation. The high viscosity of gel originating from the polymeric mixed-metal species in solution prevents the separation of precursor components and provides a uniformity of film composition. At the second stage, thermal decomposition (Equation (1) [12]) of deposited precursor occurs in the whole volume of the thin film, simultaneously resulting in randomly

oriented NaLnF₄ nanocrystals (Figure 12a). In addition, the amorphous precursor layer provides exceptional smoothness to the resulting film at lower temperatures.

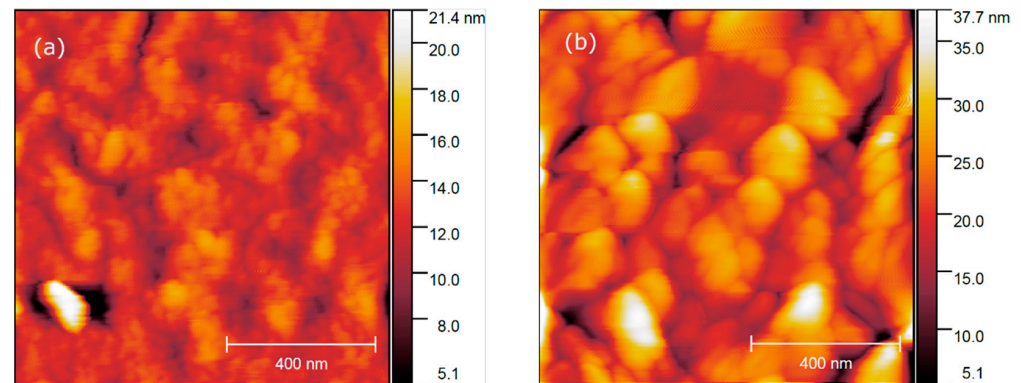
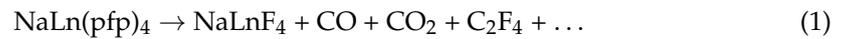


Figure 12. AFM height profiles of fluoride thin films, annealed at 400 °C and 600 °C (a) and (b), respectively.

Further AFM study of film morphology reveals that films after 400 °C annealing consist of 40–70 nm nanocrystals, which corresponds to the limited kinetics of the crystallization process at low temperature. The MOCSD films have a lower porosity and a smoother surface (root mean square roughness $S_q = 2.7$ nm for $5 \times 5 \mu\text{m}^2$ area) than has been reported for sol–gel films (average roughness of 3.4 nm or $2 \times 2 \mu\text{m}^2$ area) [36]. However, annealing at a higher temperature, e.g., 600 °C, initiates the grain growth up to 130–180 nm in lateral size (Figure 12b) and increases the overall roughness on the film ($S_q = 26$ nm). It should be also noted that the films have an equal thickness of ca. 73 nm.

GIXRD data (Figure 13a) confirms that both thin films consist of a polycrystalline NaLnF₄ phase with a domination of cubic α -NaLnF₄. It is worth noting that unlike the powder case, the hexagonal β -NaLnF₄ appears as a minor component only in the film annealed at 600 °C. This indicates that the crystallization process in quasi-2D thin films is significantly slowed down with respect to the bulk state and further optimization of deposition conditions required for the preparation of pure β -NaLnF₄ film by MOCSD.

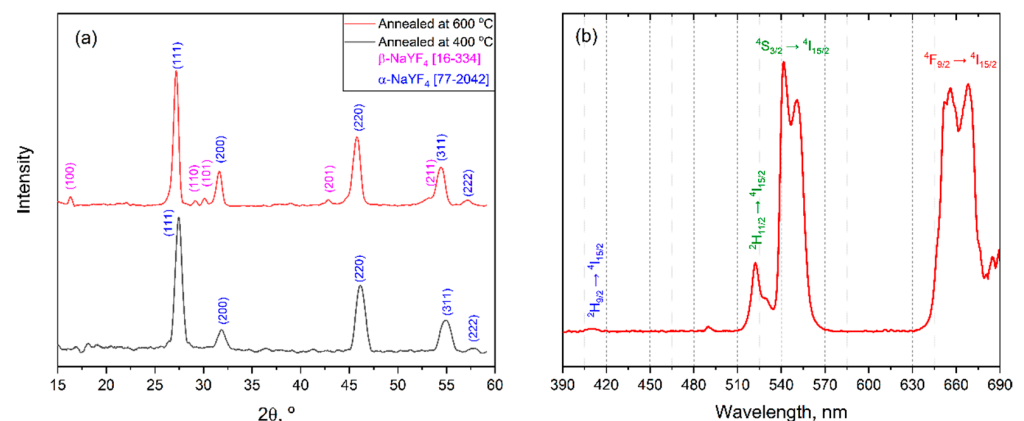


Figure 13. (a) GIXRD patterns ($\omega = 0.5^\circ$) of thin films annealed at 400 °C (black) and 600 °C (orange); (b) up-conversion luminescence spectra from thin film under 980 nm laser excitation.

Deposited thin films demonstrate an intense eye-visible up-conversion luminescence under 980 nm laser excitation despite small thickness and domination of cubic α -NaLnF₄ (Figure 13b). The emission UCL spectrum contains typical emission bands which correspond to electron transitions for the Yb³⁺-Er³⁺ system (650, 525, 550 and 420 nm: $^4F_9/2$ >

$\rightarrow |^4I_{15/2}\rangle; |^2H_{11/2}\rangle \rightarrow |^4I_{15/2}\rangle; |^4S_{3/2}\rangle \rightarrow |^4I_{15/2}\rangle; |^2H_{9/2}\rangle \rightarrow |^4I_{15/2}\rangle$, respectively [37]. It is worth noting that the relative intensities of green ($|^4S_{3/2}\rangle \rightarrow |^4I_{15/2}\rangle$) and red ($|^4F_{9/2}\rangle \rightarrow |^4I_{15/2}\rangle$) emission bands are similar to those in the UCL spectrum of β -NaY_{0.78}Yb_{0.20}Er_{0.02}F₄ film prepared by the sol-gel method [36].

4. Conclusions

Three new single-source precursors for an affordable method of fluoride film deposition were synthesized and characterized by the XRD and TG-DTA methods. According to single-crystal XRD experiments, individual lanthanide pentafluoropropionates in a crystalline state consist of isolated binuclear formula molecules Ln₂(pfp)₆(H₂O)₆ and Ln₂(pfp)₆(diglyme)₆. Substitution of water molecules for diglyme retains the binuclear molecular structure, while the later reaction with Na(pfp) results in a stable solution precursor which crystallizes to [Na₇Ln₂(pfp)₁₁(form)(diglyme)(Meac)]_∞ after organic ligand degradation. For the heterometallic complex (NaLn(pfp)₄·3H₂O), TG-DTA data confirmed the single-stage fluoride formation within a narrow temperature range, which is essential for homogeneous film deposition at low temperature. VT-PXRD study of as-obtained metal fluorides shows two phase transformations: poorly crystallized cubic NaYF₄ into hexagonal NaYF₄, and then back into a high-temperature cubic phase. Finally, the diglyme-containing single-source precursor solution allowed us to obtain a homogeneous and smooth NaLnF₄ films with an eye-visible up-conversion luminescence under 980 nm laser excitation. This work was more focused on precursor design strategy for the MOCS of complex fluorides; further optimization of film thickness and heat-treatment conditions is therefore necessary to enhance the efficiency of up-conversion.

Author Contributions: Conceptualization, D.T.; methodology, D.T., A.S. and D.G.; software, D.T., A.A.; formal analysis, D.T., A.S. and D.G.; investigation A.S., D.G., A.A. and D.B.; resources, D.T.; data curation, D.T., A.S. and D.G.; writing—original draft preparation, A.S., D.T. and D.G.; writing—review and editing, D.T. and D.G.; visualization, A.S. and D.G.; supervision, D.T.; project administration, D.T.; funding acquisition, D.T. All authors have read and agreed to the published version of the manuscript.

Funding: Artem Shevchenko acknowledges the DFG-Grant BE 7407/1-1 for funding of in situ PXRD data collection.

Institutional Review Board Statement: Not applicable.

Informed Consent Statement: Not applicable.

Data Availability Statement: The primary data presented in this study are available on request from the corresponding author.

Acknowledgments: Dmitry Tsymbarenko acknowledges support from M.V. Lomonosov Moscow State University Program of Development. Artem Shevchenko is very thankful to Sebastian Bette (Max Plank Institute for Solid State Research (MPI-FKF), Stuttgart, Germany) for his help in conducting PXRD experiments.

Conflicts of Interest: The authors declare no conflict of interest.

References

- Joubert, M.-F. Photon avalanche upconversion in rare earth laser materials. *Opt. Mater.* **1999**, *11*, 181–203. [[CrossRef](#)]
- Lui, Y.; Chem, W.; Wang, S.; Joly, A.G. X-ray luminescence of LaF₃:Tb³⁺ and LaF₃:Ce³⁺,Tb³⁺ water-soluble nanoparticles. *J. Appl. Phys.* **2008**, *103*, 063105.
- Yang, L.W.; Han, H.L.; Zhang, Y.Y.; Zhong, J.X. White Emission by Frequency Up-Conversion in Yb³⁺-Ho³⁺-Tm³⁺ Triply Doped Hexagonal NaYF₄ Nanorods. *J. Phys. Chem. C* **2009**, *113*, 18995–18999. [[CrossRef](#)]
- Zhang, P.; Chen, H.; Yang, Y.; Zhao, D.; Jia, Z.; Zheng, K.; Qin, G.; Qin, W. 3D up-conversion display of NaYF₄-PMMA co-valent-linking nanocomposites. *J. Alloys Compd.* **2018**, *753*, 725–730. [[CrossRef](#)]
- Menyuk, N.; Dwight, K.; Pierce, J.W. NaYF₄: Yb, Er—An efficient upconversion phosphor. *Appl. Phys. Lett.* **1972**, *21*, 159–161. [[CrossRef](#)]
- Tsuyoshi, K.; Yamamoto, H.; Otomo, Y. NaLnF₄:Yb³⁺, Er³⁺ (Ln: Y, Gd, La): Efficient Green-Emitting Infrared-Excited Phosphors. *J. Electrochem. Soc.* **1972**, *119*, 1561.

7. Pinol, L.; Rebello, K.; Caruso, K.; Francomacaro, A.S.; Coles, G.L. Physical vapor deposition and patterning of calcium fluoride films. *J. Vac. Sci. Technol. A* **2011**, *29*, 21001. [[CrossRef](#)]
8. Ylilammi, M.; Ranta-aho, T. Metal Fluoride Thin Films Prepared by Atomic Layer Deposition. *J. Electrochem. Soc.* **1994**, *141*, 1278. [[CrossRef](#)]
9. Jia, H.; Xu, C.; Wang, J.; Chen, P.; Liu, X.; Qui, J. Synthesis of NaYF₄:Yb–Tm thin film with strong NIR photon up-conversion photoluminescence using electro-deposition method. *CrystEngComm* **2014**, *16*, 4023–4028. [[CrossRef](#)]
10. Battiato, S.; Rossi, P.; Paoli, P.; Malandrino, G. Heterobimetallic Sodium Rare-Earth Complexes: “Third-Generation” MOCVD Precursors for the Deposition of NaREF₄ (RE = Y, Gd) Films. *Inorg. Chem.* **2018**, *57*, 15035–15039. [[CrossRef](#)]
11. Barranco, J.; Méndez-Blas, A.; Calixto, M.E. Structural, morphology and optical properties of NaYF₄ thin films doped with trivalent lanthanide ions. *J. Mater. Sci. Mater. Electron.* **2019**, *30*, 4855–4866. [[CrossRef](#)]
12. Rillings, K.; Roberts, J. A thermal study of the trifluoroacetates and pentafluoropropionates of praseodymium, samarium and erbium. *Thermochim. Acta* **1974**, *10*, 269–277. [[CrossRef](#)]
13. Hercules, D.A.; Parrish, C.A.; Saylor, T.S.; Tice, K.T.; Williams, S.M.; Lowery, L.E.; Brady, M.E.; Coward, R.B.; Murphy, J.A.; Hey, T.A.; et al. Preparation of tetrafluoroethylene from the pyrolysis of pentafluoropropionate salts. *J. Fluor. Chem.* **2017**, *196*, 107–116. [[CrossRef](#)]
14. Chen, X.; Peng, D.; Ju, Q.; Wang, F. Photon upconversion in core–shell nanoparticles. *Chem. Soc. Rev.* **2015**, *44*, 1318–1330. [[CrossRef](#)]
15. Ayadi, H.; Fang, W.; Mishra, S.; Jeanneau, E.; Ledoux, G.; Zhang, J.; Daniele, S. Influence of Na⁺ ion doping on the phase change and upconversion emissions of the GdF₃: Yb³⁺, Tm³⁺ nanocrystals obtained from the designed molecular precursors. *RSC Adv.* **2015**, *5*, 100535–100545. [[CrossRef](#)]
16. Mishra, S.; Jeanneau, E.; Bulin, A.-L.; Ledoux, G.; Jouguet, B.; Amans, D.; Belsky, A.; Daniele, S.; Dujardin, C. A molecular precursor approach to monodisperse scintillating CeF₃ nanocrystals. *Dalton Trans.* **2013**, *42*, 12633–12643. [[CrossRef](#)]
17. Grebenyuk, D.; Ryzhkov, N.; Tsymbarenko, D. Novel mononuclear mixed ligand complexes of heavy lanthanide trifluoro-acetates with diethylenetriamine. *J. Fluor. Chem.* **2017**, *202*, 82–90. [[CrossRef](#)]
18. Chen, Y.; Mishra, S.; Ledoux, G.; Jeanneau, E.; Daniel, M.; Zhang, J.; Daniele, S. Direct synthesis of hexagonal NaGdF₄ nanocrystals from a single-source precursor: Upconverting NaGdF₄:Yb³⁺, Tm³⁺ and its composites with TiO₂ for near-IR-driven photocatalysis. *Chem. Asian J.* **2014**, *9*, 2415–2421. [[CrossRef](#)]
19. Mishra, S.; Daniele, S.; Ledoux, G.; Jeanneau, E.; Joubert, M.-F. Heterometallic–complexes as novel single-source precursors for upconverting NaYF₄ co-doped with Yb and Er/Tm ions. *Chem. Commun.* **2010**, *46*, 3756–3758. [[CrossRef](#)]
20. Mishra, S.; Ledoux, G.; Jeanneau, E.; Daniele, S.; Joubert, M.-F. Novel heterometalorganic complexes as first single source precursors for up-converting NaY(Ln)F₄ (Ln = Yb, Er Tm) nanomaterials. *Dalton Trans.* **2012**, *41*, 1490–1502. [[CrossRef](#)]
21. Petříček, V.; Dušek, M.; Palatinus, L. Crystallographic Computing System JANA2006: General features. *Z. Krist.-Cryst. Mater.* **2014**, *229*, 345–352. [[CrossRef](#)]
22. Sheldrick, G.M. *SADABS V. 2.01*, Bruker/Siemens Area Detector Absorption Correction Program; Bruker AXS: Madison, WI, USA, 1998.
23. Sheldrick, G.M. *CELL_NOW*; Georg-August-Universität: Göttingen, Germany, 2008.
24. Sheldrick, G.M. *TWINABS 2012/1*; Bruker AXS: Madison, WI, USA, 2012.
25. Sheldrick, G.M. *SHELXTL*, Ver. 5.10. In *Structure Determination Software Suite*; Bruker AXS: Madison, WI, USA, 1998.
26. Tang, S.; Zhao, H. Glymes as versatile solvents for chemical reactions and processes: From the laboratory to industry. *RSC Adv.* **2014**, *4*, 11251–11287. [[CrossRef](#)] [[PubMed](#)]
27. Rohde, A.; Urland, W. Synthese, Kristallstruktur und magnetisches Verhalten von Gd(CF₃CF₂COO)₃(H₂O)₃. *Z. Anorg. Allg. Chem.* **2006**, *632*, 1141–1144. [[CrossRef](#)]
28. Tsymbarenko, D.M.; Korsakov, I.E.; Lyssenko, K.A.; Troyanov, S.I. One-dimensional coordination polymers in the crystal structures of sodium and potassium acetylacetonates. *Polyhedron* **2015**, *92*, 68–76. [[CrossRef](#)]
29. Kendin, M.; Nikiforov, A.; Svetogorov, R.; Degtyarenko, P.; Tsymbarenko, D. A 3D-coordination polymer assembled from copper propionate paddlewheels and potassium propionate 1D-polymeric rods possessing a temperature-driven single-crystal-to-single-crystal phase transition. *Cryst. Growth Des.* **2021**, *21*, 6183–6194. [[CrossRef](#)]
30. Tsymbarenko, D.; Martynova, I.; Grebenyuk, D.; Shegolev, V.; Kuzmina, N. One-dimensional coordination polymers of whole row rare earth tris-pivalates. *J. Solid State Chem.* **2018**, *258*, 876–884. [[CrossRef](#)]
31. Grebenyuk, D.; Zobel, M.; Polentarutti, M.; Ungur, L.; Kendin, M.; Zakharov, K.; Degtyarenko, P.; Vasiliev, A.; Tsymbarenko, D. A Family of Lanthanide Hydroxo Carboxylates with 1D Polymeric Topology and Ln₄ Butterfly Core Exhibits Switchable Supramolecular Arrangement. *Inorg. Chem.* **2021**, *60*, 8049–8061. [[CrossRef](#)]
32. Grebenyuk, D.; Tsymbarenko, D.; D. Synthesis and crystal structure of polymeric erbium cyclohexanecarboxylate with an unusual geometry of the polymer chain. *J. Struct. Chem.* **2022**, *63*, 3.
33. Thoma, R.E.; Hebert, G.M.; Insley, H.; Weaver, C.F. Phase Equilibria in the System Sodium Fluoride–Yttrium Fluoride. *Inorg. Chem.* **1963**, *2*, 1005–1012. [[CrossRef](#)]
34. Krämer, K.W.; Biner, D.; Frei, G.; Güdel, H.U.; Hehlen, M.P.; Lüthi, S.R. Hexagonal Sodium Yttrium Fluoride Based Green and Blue Emitting Upconversion Phosphors. *Chem. Mater.* **2004**, *16*, 1244–1251. [[CrossRef](#)]
35. Van Santen, R.A. The Ostwald step rule. *J. Phys. Chem.* **1984**, *88*, 5768–5769. [[CrossRef](#)]

36. Park, H.; Yoo, G.Y.; Kim, M.-S.; Kim, K.; Lee, C.; Park, S.; Kim, W. Thin film fabrication of upconversion lanthanide-doped NaYF₄ by a sol-gel method and soft lithographical nanopatterning. *J. Alloys Compd.* **2017**, *728*, 927–935. [[CrossRef](#)]
37. Bünzli, J.C.G.; Eliseeva, S.V. Basics of Lanthanide Photophysics. In *Lanthanide Luminescence. Springer Series on Fluorescence (Methods and Applications)*; Hänninen, P., Härmä, H., Eds.; Springer: Berlin/Heidelberg, Germany, 2010; Volume 7. [[CrossRef](#)]